JOURNAL OF MAGNETIC RESONANCE 96, 323–334 (1992)

Fast, Noniterative Shimming of Spatially Localized Signals. *In Vivo* Analysis of the Magnetic Field along Axes

ROLF GRUETTER* AND CHRIS BOESCH†

*Department of Molecular Biophysics and Biochemistry, Yale University, New Haven, Connecticut 06510; and †Magnetic Resonance Center, University and Inselspital, Inselheimmatte, CH-3010 Bern, Switzerland

Received March 27, 1991

A strategy for localized shimming is described, which is noniterating, fast, and reliable. It is shown that the magnetic field measured along a particular projection that runs through the center of a volume element can be separated into the r^n contributions from different orders n of the spherical harmonic functions. The selection of a suitable number of projections with distinctive orientations permits unambiguous determination of the coefficients of each spherical harmonic term by combining the results of polynomial regression analysis along the different axes. Shim coils are generally built to generate a field that corresponds to a single spherical harmonic. The measurement of the magnetic field along projections is used to design a rapid shim procedure that uses simple algorithms. The effect of displacing the localized volume is calculated from the representation of the spherical harmonic functions in Cartesian coordinates. The practicality and speed of the resulting method are demonstrated on a 2.35 T 40 cm bore system for the adjustment of the X, Y, Z, Z^2, and $X^2 - Y^2$ coils.

Shimming is technically achieved with several shim coils, where each is designed such that its field distribution is associated with one particular spherical harmonic function centered at the magnet origin (*1*). One-shot localization techniques, e.g., STEAM (*2*), can be used for spatially localized shimming, which is usually performed by maximizing the envelope of the FID or echo, resulting in an iterating and thus relatively time-consuming adjustment. A disadvantage of these techniques is that the result may depend on operator skills as well as on the starting conditions. Localization of the signal allows the measurement at positions away from the magnet center, where the different shim coils interact. An adjustment by FID methods then becomes hopelessly difficult if other than the X, Y, and Z shim coils are used (*3*). Consequently, most *in vivo* shimming has been restricted to use of these three coils. In many situations, however, there may be a need to correct for higher-order inhomogeneities present in the volume under investigation. Alternative methods have been described [e.g., (*4, 5*)] which utilize knowledge of the field generated by the shim coils. These methods measure the magnetic field in several planes about the magnet center, which generally results in time-consuming data acquisition. Furthermore, the mathematical treatment that is involved is rather complex (matrix inversion) and usually not easily modified for locally restricted homogeneity adjustments.

It is the purpose of this paper to demonstrate that it is sufficient to measure the magnetic field along linear projections through the center of the localized volume.

0022-2364/92 $3.00

Experimental time is thereby significantly reduced and simple mathematical formulas can be used to compute the changes in shim currents. Moreover, the method yields an analytical and quantitative characterization of the magnetic field at a given position in terms of spherical harmonics. The effect of displacement of the volume on the correction currents in the shim coils is also demonstrated. The practicality of the suggested procedure for *in vivo* spectroscopy is demonstrated by the implementation of the adjustment of the X, Y, Z, Z^2, and $X^2 - Y^2$ coils on a 2.35 T magnet with a 40 cm bore.

METHODS USED TO MEASURE THE MAGNETIC FIELD

The experimental shim procedure was initially implemented on a 2.35 T magnet (MEDSPEC 24/40, Bruker-Spectrospin, Fällanden, Switzerland) with a 40 cm room-temperature bore and 35 cm free access (*6*), which was equipped with 15 room-temperature shim coils [$Z^0, X, Y, Z, Z^2, X^2 - Y^2, ZX, ZY, 2XY, Z^3, Z^2X, Z^2Y, Z(X^2 - Y^2), Z(2XY), Z^4$] and a gradient preemphasis as well as a Z^0 compensation unit to reduce eddy-current effects. A homebuilt double-tuned probe head was used for RF transmission and reception (*7*).

Preliminary results with the shim strategy suggested in this paper have also been obtained in phantom solutions with surface coils in a 2.1 T whole-body Biospec magnet (Oxford Research Systems, Billerica) with 60 cm free access, which was equipped with the same number of shim coils.

The magnetic field was measured along bars by calculating the phase along projections that were obtained with the stimulated-echo sequence (*2*) shown in Fig. 1. The

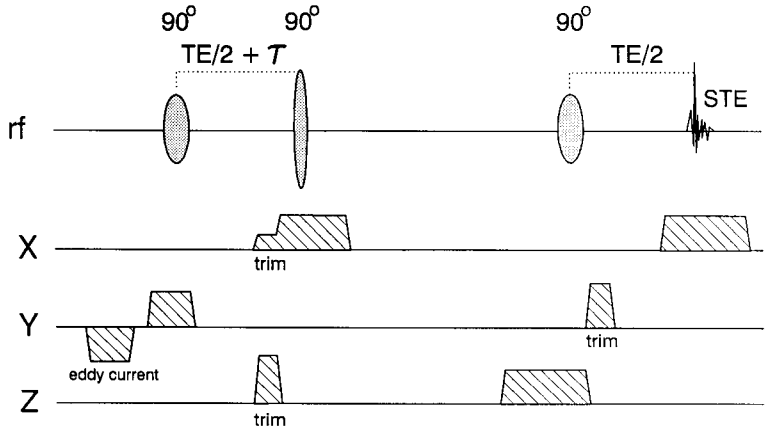

FIG. 1. Sequence used to localize the signal along the bar. The stimulated echo (*2*) is recorded in the presence of a read gradient for one-dimensional space encoding. The broadbanded second pulse was a sinc pulse (5 kHz bandwidth) used to reduce the bar length to 3.7 cm. The first and third pulses were Gaussian shaped (1 kHz bandwidth) and used to determine the bar width, which was set to 1.3 cm. The gradient trim pulses were used to rephase the stimulated echo and to dephase other echoes. The first y gradient pulse was added to reduce residual eddy-current effects during the extra delay τ, which was added every second scan. The specific gradients shown here were used to localize a bar parallel to the magnet x axis. Other orientations were generated by using different sets of orthogonal gradient orientations.

two narrow-banded, slice-selective pulses (first and third pulses in Fig. 1) and concomitant gradients determined the position and orientation of the bar. A broadband sinc pulse was used in the third direction to reduce the echo amplitude by limiting the length of the bar. The length of the bar was 3.7 cm and the width was set to 1.3 cm. The echo delay between the first and second pulse was varied by τ on alternate scans and corresponding echoes 1 and 2 were stored in different memory blocks. Eddy-current effects during this extra delay τ were minimized to a negligible level using previously established procedures (*8*). The difference of the phases $\Delta\varphi = \varphi^{(1)} - \varphi^{(2)}$ of the projections obtained with and without the extra delay τ yielded the frequency $\Delta\nu = \Delta\varphi/2\pi\tau$, which is related to the magnetic field through the gyromagnetic ratio. To eliminate errors in the frequency calculation, the phase difference between consecutive digitized points along the projection was kept well below π by zero-filling the acquisition time of 5 ms to 40 ms prior to the Fourier transformation. The discontinuities resulting from the use of the arctan function were eliminated with a simple algorithm that defined intervals free from discontinuities, within which the same multiple of π was added or subtracted, respectively.

If enough S/N was available, one acquisition per direction and τ value was sufficient, resulting in a total experimental time of a few seconds. We used a repetition time of 2.5 s, where eddy-current effects between successive scans have died away to a negligible level. In addition, we preferred to acquire after two dummy scans and to repeat the acquisition at least once in order to eliminate spurious echoes. This procedure resulted in an experimental time of typically 15–25 s per spatial orientation.

To assess the effect of the homogeneity adjustment, the magnetic field was imaged with a previously published stimulated-echo imaging sequence (*8*) that was modified by varying the first echo delay by 15 ms, similar to the sequence in Fig. 1.

THEORY

Shim coils are designed to produce a magnetic field distribution in space that corresponds to one particular spherical harmonic function centered at the magnet origin (*1*). Therefore, after a previous calibration of shim-coil currents, an analysis of a given inhomogeneity in spherical harmonics can be used to calculate the changes in the shim-coil currents that cancel the inhomogeneity. Table 1 lists the field distributions generated by the most common shim coils. However, shim coils act independently on the homogeneity only for volumes centered in the magnet. A change in the current of a shim coil produces additional lower-order terms at $r_0 = (x_0, y_0, z_0)$. The magnitude of these unwanted but unavoidable lower-order terms depends on the magnitude of the change in the higher-order coils and the location r_0 of the displaced volume (*3*).

In this section it is demonstrated that the magnetic field can be analyzed along lines that run through the center of a volume of interest. In a first step of the mathematical treatment, the position is restricted to the center of the magnet and of the shim system, respectively. Remotely located volumes are treated in a second step, because it can be shown that there is a simple relationship between the coefficients of the expansion in spherical harmonic functions in a remote volume and the coefficients of the spherical harmonics centered in the magnet, which are proportional to the currents in the shim coils.

TABLE 1

Field Generated by Low-Order Shims and Associated Spherical Harmonic Functions in Spherical and Cartesian Coordinates[a]

n	m	Shorthand notation	Coefficients[b] (k_{nm})	Spatial dependence $r^n W_{nm}(\theta, \phi)$	
				Spherical	Cartesian
1	0	Z^c	C_1	$r\cos\theta$	z
1	1	X^c	A_{11}	$r\sin\theta\cos\phi$	x
1	1	Y^c	B_{11}	$r\sin\theta\sin\phi$	y
2	0	Z^{2c}	C_2	$r^2(3\cos^2\theta - 1)/2$	z^2-$(x^2 + y^2)/2$
2	1	XZ	$3A_{21}$	$r^2\sin\theta\cos\theta\cos\phi$	xz
2	1	YZ	$3B_{21}$	$r^2\sin\theta\cos\theta\sin\phi$	yz
2	2	$X^2 - Y^{2c}$	$3A_{22}$	$r^2\sin^2\theta\cos 2\phi$	$x^2 - y^2$
2	2	$2XY$	$3B_{22}$	$r^2\sin^2\theta\sin 2\phi$	$2xy$
3	0	Z^3	C_3	$r^3(5\cos^3\theta - 3\cos\theta)/2$	$z[z^2 - 3(x^2 + y^2)/2]$
3	1	XZ^2	$\frac{3}{2}A_{31}$	$r^3\sin\theta(5\cos^2\theta - 1)\cos\phi$	$x(4z^2 - x^2 - y^2)$
3	1	YZ^2	$\frac{3}{2}B_{31}$	$r^3\sin\theta(5\cos^2\theta - 1)\sin\phi$	$y(4z^2 - x^2 - y^2)$
3	2	$Z(X^2 - Y^2)$	$15A_{32}$	$r^3\sin^2\theta\cos\theta\cos 2\phi$	$z(x^2 - y^2)$
3	2	XYZ	$15B_{32}$	$r^3\sin^2\theta\cos\theta\sin 2\phi$	$2xyz$
3	3	X^3	$15A_{33}$	$r^3\sin^3\theta\cos 3\phi$	$x^3 - 3xy^2$
3	3	Y^3	$15B_{33}$	$r^3\sin^3\theta\sin 3\phi$	$3x^2y - y^3$

[a] The constant field term Z^0 ($n = m = 0$) has been left out since this trivial field can be set to zero by adjusting the spectrometer frequency.

[b] The coefficients C_n, A_{nm}, and B_{nm} have been separated together with constant factors from the spatial dependence of the spherical harmonics (Eq. [2]), because they are lumped together by the calibration of the shim currents. The definition of A_{nm}, B_{nm}, and C_n is according to (*1*), but C_{nm} has been separated into A_{nm} associated with $\cos(m\phi)$ and B_{nm} with $\sin(m\phi)$.

[c] Shims whose currents were adjusted in the implemented experimental demonstration of the method.

Magnetic field analysis along axes. Any static magnetic field B can be written as a sum of spherical harmonics (*1*), e.g., as

$$B(r, \theta, \phi) = \sum_n [T_n + \sum_m (T^s_{nm} + T^c_{nm})], \qquad [1]$$

where

$$T_n = C_n r^n P_n(\cos\theta) = k_n r^n W_n(\theta)$$

$$T^s_{nm} = B_{nm} r^n P_{nm}(\sin\theta)\sin m\phi = k^s_{nm} r^n W^s_{nm}(\phi, \theta)$$

$$T^c_{nm} = A_{nm} r^n P_{nm}(\sin\theta)\cos m\phi = k^c_{nm} r^n W^c_{nm}(\phi, \theta). \qquad [2]$$

The definition of A_{nm}, B_{nm}, and C_n is according to (*1*), but we separated C_{nm} in Ref. (*1*) into the term A_{nm} associated with $\cos(m\phi)$ and B_{nm} associated with $\sin(m\phi)$. For the definition of the Legendre functions P_n (and associated P_{nm}), see (*1*). A list of these functions together with the definition of k_n, k^s_{nm}, k^c_{nm}, W_n, W^s_{nm}, W^c_{nm} is given in Table 1 for small values of m and n. It is important for the further theory of

the spherical harmonics that the radial dependence r^n (Eq. [2]) can be completely separated from the angular functions $W^{s}_{nm}(\phi, \theta)$, $W^{c}_{nm}(\phi, \theta)$, and $W_n(\theta)$.

To simplify the notation of summation and to avoid the explicit separation of sin $m\phi$ and cos $m\phi$ we use for a *given order n* a single index i ($i = 1 \cdots M$) for all angular functions and corresponding coefficients. M represents the number of spherical harmonics associated with r^n and in the summation $i = 1 \cdots M$, M may vary for different n; i.e., the W_{ni} represent W_n, W^{s}_{n1}, W^{c}_{n1}, etc., and the k_{ni} represent k_n, k^{s}_{n1}, k^{c}_{n1}, etc. In this simplified notation, Eq. [1] can now be written as

$$B(r, \theta, \phi) = \sum_n \{ r^n \sum_i [k_{ni} W_{ni}(\phi, \theta)] \}. \quad [3]$$

Along a straight line that runs through the center of the coordinate system, the angles θ and ϕ do not vary and, consequently, all W_{ni} are constant. From Eqs. [2] and [3] it is clear that the magnetic field along any given straight line through the coordinate center, denoted by the index j, with the orientation given by $[\phi^{(j)}, \theta^{(j)}]$ can be written as a polynomial function of r with the coefficients $p_n^{(j)}$:

$$B[r, \theta^{(j)}, \phi^{(j)}] = \sum_n [r^n p_n^{(j)}] = \sum_n \{ r^n \sum_i [k_{ni} W_{ni}^{(j)}] \}. \quad [4]$$

$W_{ni}^{(j)} \equiv W_{ni}[\theta^{(j)}, \phi^{(j)}]$ is constant along the projection j and describes the contribution of spherical harmonic i with an r^n dependence to the projection along the axis j. The values of $W_{ni}^{(j)}$ for some selected axes are listed in Table 2. By equating polynomial coefficients on both sides in Eq. [4], we obtain the exact relationship

$$p_n^{(j)} = \sum_i [k_{ni} W_{ni}^{(j)}]. \quad [5]$$

The experimental determination of the magnetic field along the projection j—which is characterized by the pair $[\theta^{(j)}, \phi^{(j)}]$—and the subsequent polynomial regression analysis yield polynomial coefficients $a_n^{(j)}$ that are associated with an experimental error $\epsilon_n^{(j)}$; i.e.,

$$\epsilon_n^{(j)} = p_n^{(j)} - a_n^{(j)}. \quad [6]$$

Assuming this experimental error to be of Gaussian distribution, we obtain the k_{ni} by standard least-square methods from the condition $\sum [\epsilon_n^{(j)}]^2 = \min$ by setting the partial derivative with respect to k_{nl} to zero:

$$\frac{\partial}{\partial k_{nl}} \sum_j [\epsilon_n^{(j)}]^2 = 0. \quad [7]$$

By substituting $\epsilon_n^{(j)}$ with Eq. [6] and expressing $p_n^{(j)}$ with Eq. [5], we obtain for *each* order n a set of M equations,

$$\sum_j \{ \sum_i [W_{ni}^{(j)} k_{ni}] - a_n^{(j)} \} W_{nl}^{(j)} = 0 \quad [8]$$

since l runs from 1 to M, where M represents the number of nth-order spherical harmonics. These M equations can be regrouped into matrix form:

TABLE 2

Relative Contribution $W_{ni}^{(j)}$ of Shim i with an r^n Dependence along the Axis j[a]

	Orientation		Shims[b]														
			n =	1		2					3						
			m = 0	1	1	0	1	1	2	2	0	1	1	2	2	3	3
j	$\theta^{(j)}$ (degrees)	$\phi^{(j)}$ (degrees)	Z^c	X^c	Y^c	Z^{2c}	ZX	ZY	$X^2 - Y^{2c}$	$2XY$	Z^3	XZ^2	YZ^2	$Z(X^2 - Y^2)$	XYZ	X^3	Y^3
1 (z)[c]	0	—	1	0	0	1	0	0	0	0	1	0	0	0	0	0	0
2 (x)[c]	90	0	0	1	0	−1/2	0	0	1	0	0	−1	0	0	0	1	0
3 (y)[c]	90	90	0	0	1	−1/2	0	0	−1	0	0	0	−1	0	0	0	−1
4 (xy)	90	45	0	$1/\sqrt{2}$	$1/\sqrt{2}$	−1/2	0	0	0	1	0	$-1/\sqrt{2}$	$-1/\sqrt{2}$	0	0	$-1/\sqrt{2}$	$1/\sqrt{2}$
5 (yx)	90	135	0	$-1/\sqrt{2}$	$1/\sqrt{2}$	−1/2	0	0	0	−1	0	$1/\sqrt{2}$	$-1/\sqrt{2}$	0	0	$1/\sqrt{2}$	$1/\sqrt{2}$
6 (xz)	45	0	$1/\sqrt{2}$	$1/\sqrt{2}$	0	1/4	1/2	0	1/2	0	$-1/4\sqrt{2}$	$3/2\sqrt{2}$	0	$1/2\sqrt{2}$	0	$1/2\sqrt{2}$	0
7 (zx)	135	0	$-1/\sqrt{2}$	$1/\sqrt{2}$	0	1/4	−1/2	0	1/2	0	$1/4\sqrt{2}$	$3/2\sqrt{2}$	0	$-1/2\sqrt{2}$	0	$1/2\sqrt{2}$	0
8 (yz)	45	90	$1/\sqrt{2}$	0	$1/\sqrt{2}$	1/4	0	1/2	−1/2	0	$-1/4\sqrt{2}$	0	$3/2\sqrt{2}$	$-1/2\sqrt{2}$	0	0	$-1/2\sqrt{2}$
9 (zy)	135	90	$-1/\sqrt{2}$	0	$1/\sqrt{2}$	1/4	0	−1/2	−1/2	0	$1/4\sqrt{2}$	0	$3/2\sqrt{2}$	$1/2\sqrt{2}$	0	0	$-1/2\sqrt{2}$

[a] Values of the angular dependence $W_{ni}^{(j)} \equiv W_{ni}[\theta^{(j)}, \phi^{(j)}]$ of a shim i for a selected axis j with the orientation $[\theta^{(j)}, \phi^{(j)}]$ are calculated according to Eq. [2] and Table 1.

[b] The spatial dependence of the spherical harmonics (and shims, respectively) is listed in Table 1.

[c] Projections and shims that were used in the experimental implementation on the small-bore system.

$$\begin{bmatrix} \sum_j W_{n1}^{(j)2} & \cdots & \sum_j W_{n1}^{(j)} W_{nM}^{(j)} \\ \cdots & \cdots & \cdots \\ \sum_j W_{nM}^{(j)} W_{n1}^{(j)} & \cdots & W_{nM}^{(j)2} \end{bmatrix} \begin{bmatrix} k_{n1} \\ \cdots \\ k_{nM} \end{bmatrix} = \begin{bmatrix} \sum_j a_n^{(j)} W_{n1}^{(j)} \\ \cdots \\ \sum_j a_n^{(j)} W_{nM}^{(j)} \end{bmatrix}. \quad [9]$$

Equation [9] can be solved for the k_{ni} by matrix inversion if the quadratic matrix has M linear independent rows or columns, respectively. A very simple solution for the k_{ni} is obtained when the matrix in Eq. [9] is diagonal, which is the case if the orientations of the axes are chosen such that

$$\sum_j W_{na}^{(j)} W_{nb}^{(j)} \begin{cases} =0 & \text{for } a \neq b \\ >0 & \text{for } a = b. \end{cases} \quad [10]$$

The solution is then given by

$$k_{ni} = \frac{\sum_j a_n^{(j)} W_{ni}^{(j)}}{\sum_j W_{ni}^{(j)2}}. \quad [11]$$

Note that the matrix in Eq. [9] is entirely determined by the shims that are optimized and by the orientation of the axes along which the magnetic field is measured in the performed experiment. On the other hand, the experiment can be characterized entirely by the not necessarily quadratic matrix $\mathbf{W}_n$ (which is not the matrix in Eq. [9]), whose elements $(W_n)_{ij}$ are given in Eq. [3] by $W_{ni}^{(j)} \equiv W_{ni}[\theta^{(j)}, \phi^{(j)}]$. The matrix coefficients $(W_n)_{ij}$ describe the contribution of shim i with an r^n dependence along the projection j. Equation [10] implies that the orientation of the axes is chosen such that matrix $\mathbf{W}_n$ has orthogonal columns. This imposes no severe restriction on the experimental design, as can be seen from Table 2, where an example of a matrix $\mathbf{W}_n$ with elements $W_{ni}^{(j)}$ is given for a set of shim coils and axis orientations.

Experimental example. We selected the three main axes x, y, and z as projections along which to determine the shims with $n = 1$ and $n = 2$. For the linear shims X, Y, and Z ($n = 1$), $\mathbf{W}_1$ with the elements $W_{1i}^{(j)}$, defined according to Eq. [4], is a submatrix in Table 2 identical to the unity matrix. The linear coefficients $a_1^{(x)}$, $a_1^{(y)}$, $a_1^{(z)}$, that were obtained from the polynomial regression analyses along the x, y, and z axes, respectively, are obviously identical to the coefficients k_{ni} for $n = 1$:

$$k_{11} = a_1^{(x)}, \qquad k_{12} = a_1^{(y)}, \qquad k_{13} = a_1^{(z)}. \quad [12]$$

The coefficient $a_1^{(x)}$ is determined by polynomial regression from the projection along the x axis, $a_1^{(y)}$ along the y axis, and $a_1^{(z)}$ along the z axis.

For $n = 2$, the matrix $\mathbf{W}_2$ with the elements $W_{2i}^{(j)}$ for the Z^2 and $X^2 - Y^2$ shims measured along the three principal axes x, y, and z is a submatrix that can be obtained from the matrix in Table 2:

$$\mathbf{W}_2 = \begin{bmatrix} 1 & 0 \\ -\frac{1}{2} & 1 \\ -\frac{1}{2} & -1 \end{bmatrix}. \quad [13]$$

Table 2 shows that the shims $2XY$, ZX, and ZY are not determined from this experiment, because their contribution along the principal axes are zero; i.e., their matrix columns $W_{2i}^{(j)}$ vanish and they have therefore not been included in Eq. [13]. Because the columns of $W_{2i}^{(j)}$ are orthogonal (Eq. [10]), we can use Eq. [11] for the calculation of the coefficient k_{21} of the Z^2 and k_{22} of the $X^2 - Y^2$ shims:

$$k_{21} = \frac{2a_2^{(z)} - a_2^{(x)} - a_2^{(y)}}{3} \qquad [14]$$

$$k_{22} = \frac{[a_2^{(x)} - a_2^{(y)}]}{2}. \qquad [15]$$

Here, $a_2^{(x)}$ is the quadratic coefficient of the polynomial regression along the x axis, $a_2^{(y)}$ that along the y axis, and $a_2^{(z)}$ that along the z axis.

The effect of translation of the volume. In the above theoretical analysis we assumed the center of the coordinate system to coincide with that of the magnet and the shim-coil system, which is useful for a direct calculation of the shim currents only for those volumes that are centered at the magnet's isocenter. For spatially remote volumes the origin of the coordinate system is shifted relative to that of the magnet and the shim correction currents must take this shift into account as pointed out by Hoult (*3*). The analysis of the spatial field distribution in terms of spherical harmonics, however, can still be performed as if the volume were located at the magnet center. The new coordinate system (x', y', z') is centered at the position (x_0, y_0, z_0) in magnet coordinates, with the relationships

$$x' = x - x_0, \qquad y' = y - y_0, \qquad z' = z - z_0. \qquad [16]$$

The corrections necessary depend on the volume position and are taken into account after the inhomogeneities are analyzed, as shown below.

For *linear* shims, the only effect of the volume center not being at the origin is to produce a frequency shift that is given for the X shim by $-x_0k_{11}$, for the Y shim by $-y_0k_{12}$, and for the Z shim by $-z_0k_{13}$. The coefficients $-k_{11}$, $-k_{12}$, and $-k_{13}$ correct for the linear inhomogeneity terms at (x_0, y_0, z_0) and are determined according to Eq. [12]. These frequency shifts can be corrected simply by adjusting the spectrometer frequency.

In order to determine the *quadratic* terms ($n = 2$) and the corresponding shim currents, no correction for the voxel position need be taken into account. However, any change in a quadratic shim coil will introduce linear terms ($n = 1$) and a frequency shift. For example, the spatial function of the Z^2 shim in Cartesian coordinates (Table 1) can be written in the shifted coordinates x', y', z' (Eq. [16]):

$$\begin{aligned} z^2 - (x^2 + y^2)/2 = {} & z'^2 - (x'^2 + y'^2)/2 \\ & - x_0x' - y_0y' + 2z_0z' \\ & + z_0^2 - (x_0^2 + y_0^2)/2. \end{aligned} \qquad [17]$$

Since the field produced by the change in current in the Z^2 coil is given by Eq. [17] multiplied by $-k_{21}$, the terms for which the linear shims must correct are $-k_{21}x_0$, $-k_{21}y_0$, and $2k_{21}z_0$, respectively. For the $X^2 - Y^2$ coil, the corresponding values are

given by $+2k_{22}x_0$ and $-2k_{22}y_0$. Similar expressions can be derived for all other coils using the notation in Cartesian coordinates as in Table 1.

It is worthwhile to note that this correction for remote voxels, i.e., the expansion of the spherical harmonics about a moved origin, is possible only if the coefficients k_{ni} are known quantitatively; e.g., FID-optimizing shim strategies fail for higher-order shims if used without extra hardware compensation (*3*).

RESULTS

To illustrate the procedure, a method was implemented that measured the static field along the three principal axes x, y, and z, respectively. The adjustment of the X, Y, Z, Z^2, and $X^2 - Y^2$ shim coils was thereby possible from Eqs. [12], [14], and [15]. It should be noted, however, that the general principles on which the method is based can be extended to include all first- and second-order shim coils, as well as higher-order shims, e.g., from Table 2 combined with Eq. [11]. This was confirmed by phantom results obtained with an initial implementation on a 2.1 T Bruker Biospec whole-body system that used all nine orientations in Table 2 (data not shown).

The field distribution of the five shim coils was imaged and found to be approximately equal to that of the corresponding spherical harmonic function. The field of each shim coil was imaged by subtracting the homogeneity of the field obtained at two different current settings of the corresponding shim power supply. The reading of the shim control monitor (SCM) was calibrated for each shim coil by measuring the change of the coefficients of the polynomial regression along the three axes at the center of the magnet while successively changing the current in one shim coil.

We implemented a procedure that consisted of the following six steps: (i) Spectrometer frequency and RF pulse gains are adjusted. (ii) Projections along the x' axis are acquired and the field variation is calculated from the phase difference along the projection. $a_1^{(x)}$ and $a_2^{(x)}$ are extracted with second-order polynomial regression that included a constant term. (iii) Step (ii) is repeated along the y' axis, yielding $a_1^{(y)}$ and $a_2^{(y)}$. (iv) Step (ii) is repeated along the z' axis, yielding $a_1^{(z)}$ and $a_2^{(z)}$. (v) The currents in the shim coils are changed according to Eqs. [12], [14], and [15] and previous calibrations. The currents in the first-order coils are then changed according to the changes in the second-order coils (Z^2 and $X^2 - Y^2$) and the position of the volume with respect to the magnet center. (vi) The spectrometer frequency is readjusted to avoid localization errors.

It is advisable to control the effectiveness of the method by repeating steps (ii) through (vi). In samples, the control measurement showed that good homogeneity was achieved in one step in those volumes whose center was not more than 2 cm away from the magnet center. At distances further out, convergence usually required two to three steps, because of a misadjustment of the X and Y coils that had to be corrected in a second step. These misadjustments seemed to stem from a deviation of the $X^2 - Y^2$ coil from its nominal field distribution. The homogeneity adjustment was independent of the starting conditions in the five shim coils as judged from the observation that a change of the current in any of the five shim coils was always returned to the optimal value within experimental error.

In Fig. 2 the magnetic field homogeneity was imaged prior to (Fig. 2A) and after automated shimming (Fig. 2B) at a position (indicated by the cross) that was offset

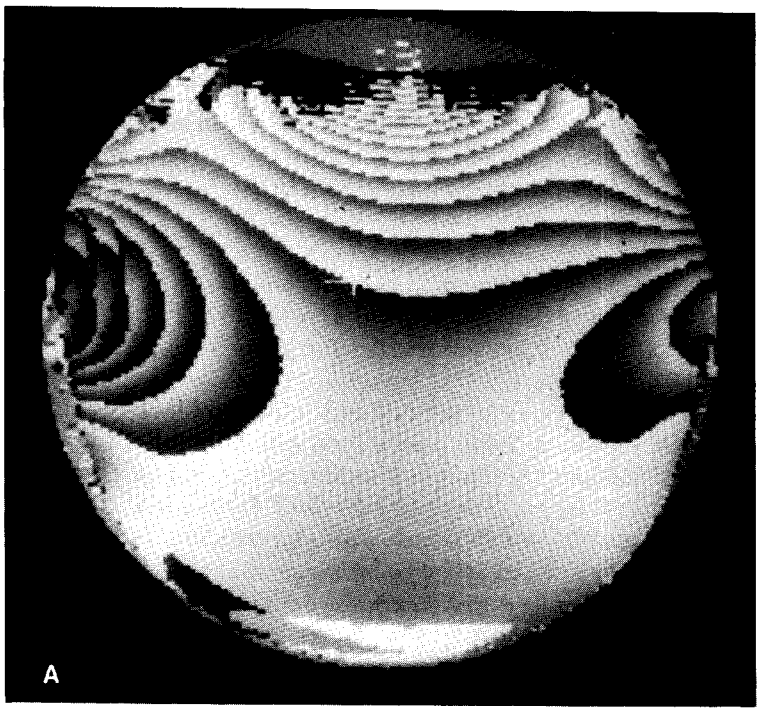
A

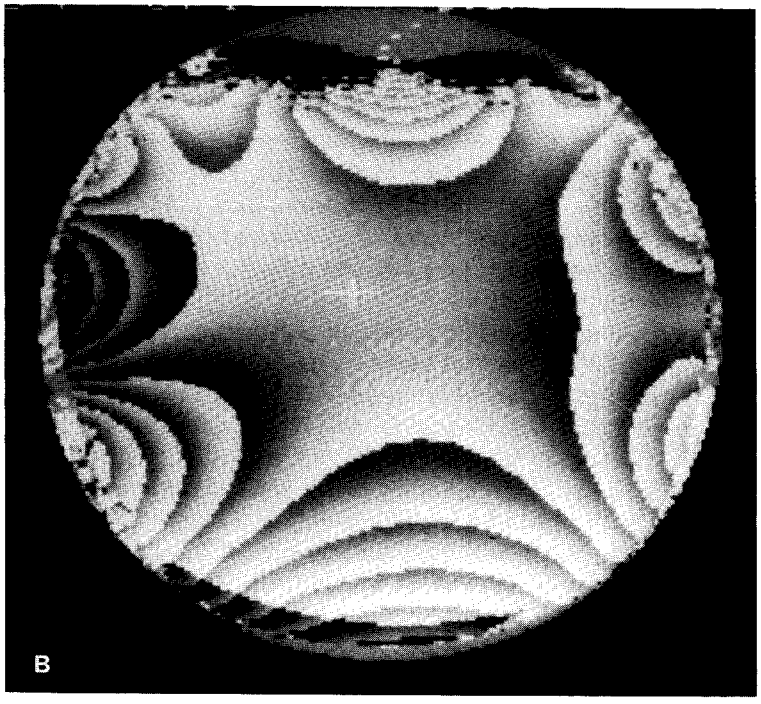
B

from the magnet center. The homogeneity improvement shown in Fig. 2B over Fig. 2A was achieved in five minutes by repeating steps (ii) to (vi) twice. The experimental time needed to go through points (ii) to (vi) was typically below three minutes, including computational time.

The same observations made in samples were repeated *in vivo*. The spectrum in Fig. 3 illustrates the excellent homogeneity that was achieved in ^{31}P-NMR spectra localized with an eddy-current-compensated ISIS sequence (*8*). The linewidth of PCr was generally between 6 and 8 Hz for 64–125 ml volumes (*9*).

DISCUSSION

A procedure has been described with which the static magnetic field distribution can be measured and analyzed considerably faster than with chemical-shift imaging methods or via microprobes. In contrast to FID shimming, the procedure can be used to shim very reliably on remote volumes with higher-order shim coils, as has been demonstrated by the excellent performance on a 2.35 T 40 cm bore system. Considering the various drawbacks present in such a small-bore system, the procedure seems to be robust against a variety of experimental imperfections. These include strong eddy-current effects (*8*), limited gradient linearity, and limited homogeneity of the static field B_0, and the possibility that the magnetic field generated by the shim coils deviates slightly from the designed theoretical distribution. These imperfections generally increase the experimental time needed for the adjustment since the procedure just must be repeated as in the case of Fig. 2. On the other hand, a systematically false adjustment of the shim coils may be obtained if care is not taken to minimize eddy-current effects during the extra echo delay τ of the sequence in Fig. 1. In addition, the linewidth may not be optimal if eddy-current effects are present during the data acquisition in the actual spectroscopic experiment, which is most likely done with a different technique, as in Fig. 3, where ISIS (*10*) was used.

The shim procedure outlined herein is restricted to situations where only one major peak is present in the proton spectrum. However, this condition can always be met by, e.g., presaturation of the unwanted resonances, if necessary. In order to provide a reliable shim adjustment, sufficient signal should be available along all parts of the projections. This will generally be the case since localized volumes are seldom placed across regions void of proton signal, e.g., across bone. However, such a situation can occur with surface coils if the pulse power has been set such that a projection runs through a region where a pulse in the sequence of Fig. 1 generates a flip angle close to 180°.

The narrow linewidths in the ^{31}P spectra obtained on the small-bore system *in vivo* (Fig. 3) and preliminary phantom results on a whole-body system indicate that the

---

FIG. 2. Images of the magnetic field show the effect of the procedure at a location distant from the magnet center. The position (cross) was displaced 3.5 cm away from the magnet center in the z direction and 1 cm away in the x direction ($y = 0$). The sample was a 12 cm diameter sphere filled with water that was displaced in the z direction by 3 cm relative to the magnet center. Both images were calculated from the difference of phase images acquired in the coronal plane ($y = 0$) with and without the extra delay τ. Discontinuities occur every 0.66 ppm. (A) The field obtained with a standard shim setting was imaged prior to the adjustment. (B) The field was imaged after localized shimming with the procedure outlined in the text that used the X, Y, Z, Z^2, and $X^2 - Y^2$ coils.

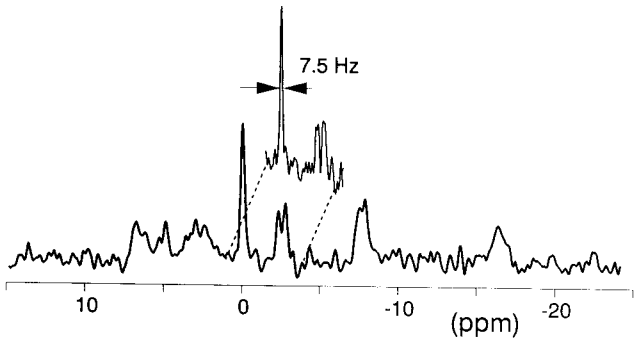

FIG. 3. Homogeneity achieved *in vivo*. The sensitivity-enhanced spectrum was obtained from a $5 \times 5 \times 5$ cm^3 volume located in the central nuclei (basal ganglia and thalamus) of a healthy six-month-old infant. The signal was acquired in 9 min (TR = 4 s, NS = 128) using an eddy-current-compensated ISIS sequence (*8, 10*). The inset illustrates the high spectral resolution of the FT obtained from the unprocessed FID.

method described here will perform even better on most whole-body systems, where instrumental imperfections are minor.

The procedure outlined here can be extended to adjust additional shim coils; for instance, adjusting all second-order shim coils in the optimization procedure would just double the experimental time if the homogeneity measurement is performed along the six side diagonals of the cube, as suggested in Table 2. Adjusting third- and higher-order shim coils is possible by fitting higher-order polynomials to the projections. However, for the volume size typically under investigation, this might be unnecessary.

ACKNOWLEDGMENTS

The authors thank Dr. E. Martin and Professor R. G. Shulman for the kind permission to use their systems and Dr. Ch. Fusch for the help with the *in vivo* measurements.

REFERENCES

1. F. ROMEO AND D. I. HOULT, *Magn. Reson. Med.* **1,** 44 (1984).
2. J. FRAHM, K. D. MERBOLDT, AND W. HAENICKE, *J. Magn. Reson.* **72,** 502 (1987).
3. D. I. HOULT, *J. Magn. Reson.* **73,** 174 (1987).
4. M. G. PRAMMER, J. C. HASELGROVE, M. SHINNAR, AND J. S. LEIGH, *J. Magn. Reson.* **77,** 40 (1988).
5. J. TROPP, K. A. DERBY, C. HAWRYSKO, S. SUGIURA, AND H. YAMAGATA, *J. Magn. Reson.* **85,** 244 (1989).
6. CH. BOESCH AND E. MARTIN, *Radiology* **168,** 481 (1988).
7. R. GRUETTER, CH. BOESCH, M. MÜRI, E. MARTIN, AND K. WÜTHRICH, *Magn. Reson. Med.* **15,** 128 (1990).
8. CH. BOESCH, R. GRUETTER, AND E. MARTIN, *Magn. Reson. Med.*, **20,** 268 (1991).
9. R. GRUETTER, E. MARTIN, AND CH. BOESCH, Abstracts of the Society of Magnetic Resonance in Medicine, 9th Annual Meeting, New York, p. 1002, August 18–24, 1990.
10. R. J. ORDIDGE, A. CONNELLY, AND J. A. B. LOHMAN, *J. Magn. Reson.* **66,** 283 (1986).